



1 **Short communication: Potential of Sentinel 1 InSAR and offset**  
2 **tracking in monitoring post-cyclonic landslides activities in**  
3 **Reunion Island.**

4 Marcello de Michele<sup>1</sup>, Daniel Raucoules<sup>1</sup>, Claire Rault<sup>2</sup>, Bertrand Aunay<sup>2</sup> and Michael  
5 Foumelis<sup>1,3</sup>

6 <sup>1</sup>BRGM, Geophysical Imagery and Remote Sensing Unit, Orleans, 45000, France.

7 <sup>2</sup>BRGM, Direction de Actions Territoriales, Saint Denis, La Réunion, 97400, France.

8 <sup>3</sup>Aristotle University of Thessaloniki, Department of Physical and Environmental Geography, 541 24  
9 Thessaloniki, Greece.

10 *Correspondence to:* Marcello de Michele (m.demichele@brgm.fr)

11

12 **Abstract**

13 This study examined the results of an interferometric Synthetic Aperture Radar (InSAR) and SAR Offset Tracking  
14 (OT) study on Cirque de Salazie (CdS), Reunion Island, France, within the context of the RENOVRIK project,  
15 a multidisciplinary programme to study the cyclonic risks in the South-West Indian Ocean. CdS is one of the  
16 denser populated areas in Reunion Island. One of the aims of the project was to assess whether Sentinel 1 SAR  
17 methods could be used to measure landslide motion and/or accelerations due to post cyclonic activity on CdS. We  
18 concentrated on the post 2017 cyclonic event. We used the Copernicus Sentinel 1 data, acquired between  
19 30/10/2017 and 06/11 2018. Sentinel 1 is a C-band SAR, and its signal can be severely affected by the presence  
20 of changing vegetation between two SAR acquisitions, particularly in CdS, where the vegetation canopy is well  
21 developed. This is why C-band radars such as the ones onboard Radarsat or Envisat, characterized by low  
22 acquisition frequency (24 and 36 days, respectively), could not be routinely used on CdS to measure landslide  
23 motion with InSAR in the past. In this study, we used InSAR and OT techniques applied to Sentinel 1 SAR. We  
24 find that C-band SAR onboard Sentinel 1 can be used to monitor landslide motion in densely vegetated areas,  
25 thanks to its high acquisition frequency (12 days). OT stacking reveals a useful complement to InSAR, especially  
26 in mapping fast moving areas. In particular, we can highlight ground motion in the Hell-Bourg, Ile à Vidot, Grand  
27 Ilet, Camp Pierrot, and Bellier landslides.

28

29 **1. Introduction and study area**

30 Landslide and erosion processes are causes of major concern to population and infrastructures on Reunion Island.  
31 These processes are led by the tropical climate of the island. The hydrological regime of the rivers is distinct owing  
32 to the coexistence of several major parameters that predispose it to extreme vulnerability. Holding almost all the  
33 world records for rainfall between 12 h (1170 mm) and 15 days (6083 mm), the island has a marked relief with a  
34 peak at 3,069 m, with exceptional cliffs that reach 1500 m in height.

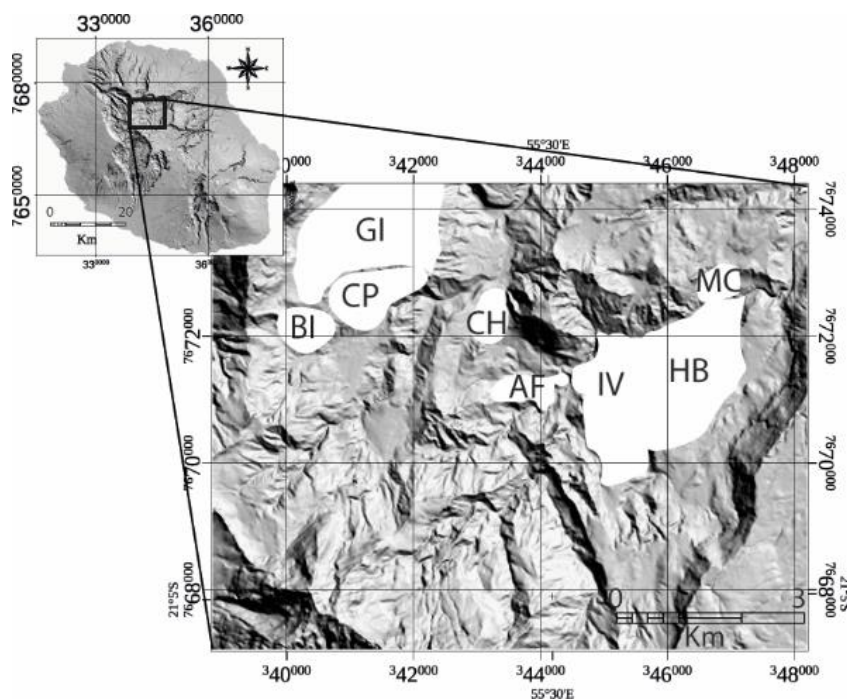


35 CdS is the rainiest of the large erosional depressions on Reunion Island (Pohl et al., 2016) with an average annual  
36 cumulative rainfall of approximately 3,100 mm since 1963; a minimum of 698 mm was recorded in 1990, and a  
37 maximum of 5,893 mm was recorded in 1980.

38 This depression is surrounded by steep rock cliffs and filled with epiclastic material. Intense river erosion incises  
39 deep valleys and has produced several isolated plateaus across the cirque.

40 The morphology, geology, and climate make CdS prone to erosion and ground movements. At least 19% of its  
41 slope has been affected by landslides (Rault et al., 2022). The active landslides range from a large slow-moving  
42 landslide of hundred million cubic meters to rapid and catastrophic slope failure with a volume exceeding one  
43 million cubic meters.

44 Eleven slow moving landslides are identified in CdS (Figure 1). Their displacement rates range from a few cm/yr  
45 to 1.15 m/yr and can accelerate after intense rainfall events, particularly because of cyclonic activity (e.g Belle  
46 et al., 2014). These landslides are commonly observed on plateaus. They cover areas that vary from tens of thousands  
47 of square m to several square km. Hell-Bourg (HB) and Grand-Ilet (GI) are the largest inhabited slow-moving  
48 landslides in the cirque with volumes of  $225 \times 10^6 \text{ m}^3$  and  $215 \times 10^6 \text{ m}^3$ , respectively (e.g. Rault et al, 2022).



49  
50 **Figure 1. Map of the study area. Slow moving landslides in the area, from existing catalogues, are highlighted in white.**  
51 **MC : Mare à citron, HB: Hell-Bourg, IV: Ilet à Vidot, AF: Affouche, CH: Chemin Henry, BL: Bellier, CP: Camp**  
52 **Pierrot, and GI: Grand-Ilet.**

53



54 Slow-moving landslides can trigger secondary landslides along their steep scarps that eventually border rivers,  
55 leading to increased solid loads. Therefore, slow-moving landslides are not only responsible for significant damage  
56 to houses and infrastructure but are also involved in the formation of torrential flows and river dams (Liébault et  
57 al. 2010, Tulet et al., 2021). Thus, understanding their kinematics/dynamics is essential for hazard and risk  
58 mitigation at the scale of Reunion Island.

59 SAR methods demonstrated useful in highlighting landslides kinematics from space (e.g. Aslan et al., 2020 –and  
60 references therein). While C band SAR can be used to comprehensively measure ground displacement, the study  
61 area is particularly challenging for C band SAR since it is densely vegetated. In this study, we test whether InSAR  
62 and OT techniques can be used to measure landslide kinematics in densely vegetated areas. Both techniques require  
63 temporal signal coherence and therefore are usually not adapted densely in vegetated areas. Particularly, C-band  
64 SAR signal can be severely affected by the presence of changing vegetation between two SAR acquisitions,  
65 particularly in CdS, where the vegetation canopy is well developed. This is why C-band radars such as the ones  
66 onboard Radarsat or Envisat, characterized by low acquisition frequency (24 and 36 days, respectively), could not  
67 be routinely used on CdS to measure landslide motion with InSAR in the past. This limitation can be palliated  
68 under certain circumstances, for instance improving repetition frequency between two or more satellite  
69 acquisitions. In this study, we exploit the improved repetition frequency of Sentinel-1 SAR to test InSAR and OT  
70 techniques in CdS after a cyclonic event in 2018. If successful, this study can serve as a demonstrator.

71

## 72 1.1 Past studies regarding ground motion from space in CdS

73 Few studies have used spaceborne remote sensing techniques to report on ground instabilities in CdS. Delacourt  
74 *et al.* (2009) used a combination of optical (Spot 5 and aerial imagery) and synthetic aperture radar (SAR) data  
75 (JERS-1 and Radarsat data) to measure ground motion on the Hell Bourg landslide. They applied the two  
76 techniques to assess their performance and quantify ground motion associated with this landslide. They found an  
77 average displacement of approximately 0.5 m/yr from 1997–2002. Le Bivic *et al.* (2017) used two pairs of ortho-  
78 rectified SPOT-5 images at 2.5 m resolution on the Hell Bourg landslide. The first pair of images spanned the  
79 period between 2002 and 2005. The second pair of images spanned the period 2006–2008. They reported that  
80 during 2002–2005, the OT method yielded ground motion within the signal noise; they deduced that landslide  
81 activity was low. From 2006–2008, they measured a maximum displacement of  $8.5 \pm 2$  m (possibly due to the  
82 storm Gamede).

83 Raucoules *et al.* (2016) used high resolution X-band SAR data from the TerraSAR-X satellite from 2010–2011.  
84 They combined ascending and descending OT maps to extract the three dimensional displacement field of the HB  
85 and GI landslides. They reported that ground displacement reached  $1 \pm 0.25$  m/y vertically and  $0.65 \pm 0.25$  m/y  
86 horizontally. They also used InSAR combined with X-band data from the Cosmo-SKYMED satellite to measure  
87 centimetric displacements on the borders of the HB and GI landslides. The X-band InSAR signal was incoherent  
88 elsewhere.

89 Raucoules *et al.* (2018; 2020) used space-borne high-resolution L-band SAR (ALOS-2/PALSAR2 data in  
90 StripMap SM1 mode) both with interferometric synthetic aperture radar (InSAR) and OT. They derived two  
91 components of the displacement field for the HB landslide. The displacement reached approximately 1 m/y from



92 2014–2016. They reported that L-band SAR performed significantly better than the C-band SAR available at the  
93 time of the study.

94

### 95 **1.2 Aim of this study**

96 Landslides displacement rates in CdS can accelerate after intense rainfall events, particularly during cyclonic  
97 activity. Their kinematic might change during such extreme events; new landslides might appear. Global  
98 Positioning System (GPS) in the study area yields precise time series at the measurement stations. SAR methods  
99 are potentially able to spatialize the ground motion information and might reveal ground motion in unexpected  
100 areas. The aim of this study is to assess whether Sentinel 1 SAR methods – both InSAR and OT- could be used to  
101 measure landslide motion and accelerations caused by post cyclonic activity in a densely vegetated area such as  
102 CdS. This study complements the one by Raucoules *et al.* (2018, 2020), who used L-band InSAR and OT to  
103 measure ground motion in CdS. The measurement of ground motion with C band SAR in densely vegetated areas  
104 is challenging because the radar waves interact with the vegetation canopy and may yield an incoherent InSAR  
105 signal if temporal changes occur between the two SAR scenes. Therefore, InSAR signal coherence largely depends  
106 on the revisit time of the satellite. The shorter the revisit time is, the higher the InSAR signal coherence, and the  
107 faster the ground motion has to be in order to be measured by InSAR. The history of C-band SAR data over la  
108 Réunion island is non-linear. The European Space Agency (ESA) Earth Remote Sensing Satellite (ERS-1 and ERS-  
109 2) SAR platforms did not cover La Réunion Island owing to orbit incompatibilities. The Canadian Space Agency  
110 Radarsat 1-2 has flown over la Réunion, but they acquired data every 24 days (Delacourt *et al.*, 2009), which  
111 makes the InSAR signal incoherent in densely vegetated areas such as the CdS. Similarly, the ESA Advance SAR  
112 (ASAR) sensor onboard the ENVISAT satellite acquired data every 35 days. Therefore, the SAR interferometric  
113 signal was incoherent for this C-band radar with a quasi-monthly repeat cycle. The Copernicus Sentinel 1 satellite  
114 can resolve these problems. Sentinel 1 hosts a C-band SAR (wavelength = 5.5 cm) whose interferometric signal is  
115 usually incoherent over densely vegetated areas; however, the high repetition frequency of Sentinel 1 (12 days in  
116 La Réunion, 6 days in mainland Europe until 2021) makes the InSAR signal potentially suitable for measuring  
117 land displacements in densely vegetated areas (e.g. Aslan *et al.*, 2020). It could be complementary or alternative  
118 to L-band SAR interferometry (Delacourt *et al.*, 2009; Raucoules *et al.* 2020) and *in-situ* techniques in La Réunion.

119

### 120 **1.3 InSAR and Offset Tracking techniques**

121 In this study, we designed the experiment as follows. We applied two SAR methods, InSAR and OT. These two  
122 methods could be complementary because InSAR can measure slow moving landslides, typically a small fraction  
123 of the employed wavelength, while OT could measure large ground motions, higher than the pixel size of the SAR  
124 scene. In contrast, OT may be limited in the measurement of small ground motions, depending on the pixel size,  
125 because the nominal lower bound precision is  $1/10^{\text{th}}$  of the pixel size of the image employed on a single  
126 correlogram.

127 InSAR methods rely on the measurement of the changes in SAR phases among multiple SAR scenes using  
128 interferometric processing (e.g. Massonnet and Feigl, 1998). It is a widely used methodology to measure ground  
129 displacements from space, in many disciplines related to tectonics (e.g. Elliot *et al.*, 2020), volcanology (e.g.



130 Doubre et al., 2017) and gravitational failures (e.g. Aslan et al., 2020). Here, we used the stacking procedure  
131 implemented in the Gamma processing chain. The stacking procedure combines multiple SAR scenes and yields  
132 ground displacement rate in the form of ground velocity map. It is used to estimate the linear rate of differential  
133 phase starting from a set of unwrapped differential interferograms. The individual interferogram phases are  
134 weighted by the time interval in estimating the phase rate. The underlying assumption is that atmospheric statistics  
135 are stationary for the set of interferograms.

136 OT is a sub-pixel image correlation technique. This technique matches two or more images at each point on a grid,  
137 analyzing the degrees of local correlation at each step. Differences in the local instantaneous frequency of the  
138 images result in sub-pixel spatial differences in ground patterns. Measurements must be performed with subpixel  
139 accuracy because the amplitude of the ground displacement is often lower than the resolution of the images,  
140 depending on the sensor used.

141 Sub-pixel image correlation technique for measuring ground surface displacements can be applied to optical (e.g.  
142 Michel et al., 1999; de Michele and Briole, 2007) and SAR amplitude images (e.g. Michel and Rignot, 1999; de  
143 Michele et al., 2010a, 2010b). The main differences between optical and SAR images are caused by the oblique  
144 SAR acquisition geometry. Therefore, instead of having east-west and north-south offsets as in optical OT, SAR  
145 OT has with slant range and azimuth offsets. Slant range is the line of sight (LOS) direction, or look angle of the  
146 satellite. The azimuth is the flying direction of the satellite (nominally 98° for Sentinel 1; nearly north-south).  
147 Moreover, azimuth offsets are «topography free», and slant range offsets are calculated in the LOS and, therefore,  
148 contain a contribution from vertical offsets, depending on the viewing angle. Thus, OT yields two components of  
149 the deformation field for one SAR scene. For details on this methodology, please refer to Michel & Rignot (1999)  
150 and Michel et al., (1999), who used it with shuttle imaging radar (SIR-C) ERS radar amplitude images, and  
151 Raucoules et al. (2013), who applied the OT method to multi temporal SAR images at La Vallette landslide. The  
152 OT technique provides a measurement of the ground displacement from the analysis of the geometrical  
153 deformation between the two SAR amplitude images. Usually SAR images with a small baseline are chosen to  
154 reduce the stereoscopic effect and geometric decorrelation. For Sentinel 1, the orbit tubes are steered within 100  
155 m maximum. Therefore, the topographic contribution to the OT in the LOS direction is negligible. In this study,  
156 we estimated the range and azimuth offset fields using cross correlation optimization of the input intensity images.  
157 This algorithm was implemented in the GAMMA software with the name of “offsets tracking” (e.g. Strozzi et al.,  
158 2002). GAMMA is a standard SAR processing software, which results have been validated among other available  
159 SAR processing chains (e.g. Raucoules et al., 2009).

160

## 161 **2. Data and processing steps**

162 At the time of this study experimental design, the Sentinel-1 mission comprised a constellation of two polar-  
163 orbiting satellites, operating day and night, hosting a C-band synthetic aperture radar, enabling them to acquire  
164 imagery regardless of the weather. We used 26 Sentinel 1 data in descending, stripmap mode, acquired every 12  
165 days from October 30, 2017, to November 06, 2018. Sentinel 1 data are provided by the European Space Agency,  
166 within the Copernicus Program of the European Union. Technically, we downloaded them as Single Look  
167 Complex (SLC) data from the Copernicus Scientific Data Hub (<https://scihub.copernicus.eu>). We did not use the



168 ascending mode, as it is less sensitive to ground motion in CdS given the SAR shadow and the unfavorable relative  
169 geometry between the SAR orbit and ground motion (e.g. Raucoules et al., 2020).

170 First, we co-registered the SAR data. Then, we created differential interferograms with data pairs spanning 12 days  
171 intervals. The topographic contribution to the interferometric phase was modelled using a DEM from the Shuttle  
172 Radar Topography Mission (SRTM). We unwrapped the differential interferograms with the minimum cost flow  
173 algorithm (Constantini, 1998). Depending on the water vapor content in the air, there may be an interferometric  
174 phase delay due to the SAR signal crossing multiple tropospheric layers. To a first approximation, this delay is  
175 proportional to the topographic slope. Therefore, we corrected the tropospheric contribution to the interferometric  
176 phase by linear regression with the DEM. At this point, we performed the stacking procedure, producing a velocity  
177 map. Then, we orthorectified the velocity map. The results are shown in Figure 2.

178 For the OT procedure, we began from the co-registered SAR data. Instead of the phases, we used the amplitude of  
179 the SAR signal and extracted multi look complex images (MLI) for each acquisition date. Multi look processing  
180 degrades the image resolution but reduces the image speckle. Because OT sensitivity to ground motion depends  
181 on the pixel resolution, we required a tradeoff between image noise and multi looking. For this study, our choice  
182 was multi looking with a factor of 3 in azimuth and 2 in range directions. This led to pixel sizes of 8.2 m in the  
183 azimuth direction and 7.9 m in the range directions. We used a correlation window of 128X128 pixels and searched  
184 for 1024 measures in range and azimuth respectively. The OT technique is nominally less affected by temporal  
185 signal decorrelation than the InSAR technique. Therefore, we used all possible image couples, leading to the  
186 creation of 351 correlograms in both range and azimuth directions. Then, we applied a stacking procedure to create  
187 one velocity map in the range direction and one in the azimuth direction. Finally, we orthorectified the results.

188

### 189 3. Results

190 We recognized and mapped three landslide areas in Salazie, active during the study period. Hell Bourg, Ilet à Vidot  
191 and an area that was considered stabilized or dormant, possibly corresponding to Crete de Salazie.

192 Hell Bourg and Ilet a Vidot are two major inhabited compound landslides of Salazie. These landslides move  
193 continuously and typically accelerate following heavy rainfall. They occupy approximately 10% of the CdS surface  
194 area. They all stand on volcanoclastic material interpreted as volcanic debris-avalanche deposits or as debris-  
195 flow/mud-flow deposits by Rault et al. (2022). Hell Bourg is a compound landslide covering a surface of  
196 approximately 2.8 km<sup>2</sup>. Ilet a Vidot is an active plateau located northwest of Hell Bourg and covers an area of 2.3  
197 km<sup>2</sup>.

198 In the next paragraph we describe both InSAR and OT results in more details.

199

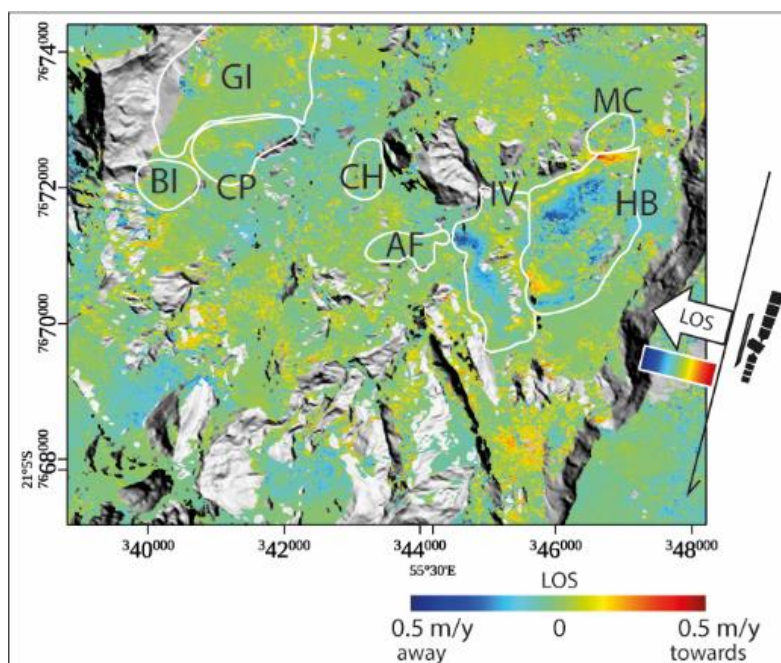
#### 200 3.1 InSAR

201 The stacking InSAR results are shown in Figure 2. They are presented as a mean velocity map, where ground  
202 motion is measured in the LOS of the satellite. InSAR is only sensitive to ground motion occurring in the LOS  
203 direction. Motion away from the satellite is represented in blue. Motion towards the satellite is represented in red.  
204 Complex combinations of those two directions of motion may lead to zero apparent motion on the InSAR velocity



205 map. From Figure 2, we observe manifold improvements with respect to velocity maps produced from former C-  
206 band InSAR missions (Delacourt *et al.*, 2009). First, we noticed that the InSAR signal was coherent over the study  
207 area, which was not expected given the densely vegetated tropical area. Second, we can see a clear pattern of  
208 ground motion in the Hell-Bourg area, approximately  $\pm 0.5$  m/yr and spatially consistent with ground observations.  
209 Figure 2 also shows ground motion on the Ilet à Vidot (IV) landslide. The InSAR signal direction on both HB and  
210 IV landslides is quite complex. This suggests the existence of complex internal landslides kinematics such as  
211 stretching of the main landslide body in HB and dismantling of IV plateau on both sides by landslides moving  
212 either eastward or westward, as expected for a compound slide and identified in the field by Rault *et al.* (2022). It  
213 also suggests a rotational component of ground motion. In this study, the InSAR signal was surprisingly coherent  
214 with a certain level of noise. We calculated the noise as  $\pm 2$  cm/yr on the InSAR velocity map. To minimize  
215 coherence loss, we used interferograms with 12 days times span only, excluding larger time-span interferograms.  
216 Owing to these limitations, we were unable to capture very slow ground motions ( $< 2$  cm/yr).

217



218

219 **Figure 2.** InSAR velocity map in the LOS of the satellite, using the descending mode. A ground displacement pattern  
220 is clearly visible in the Hell-Bourg area.

221

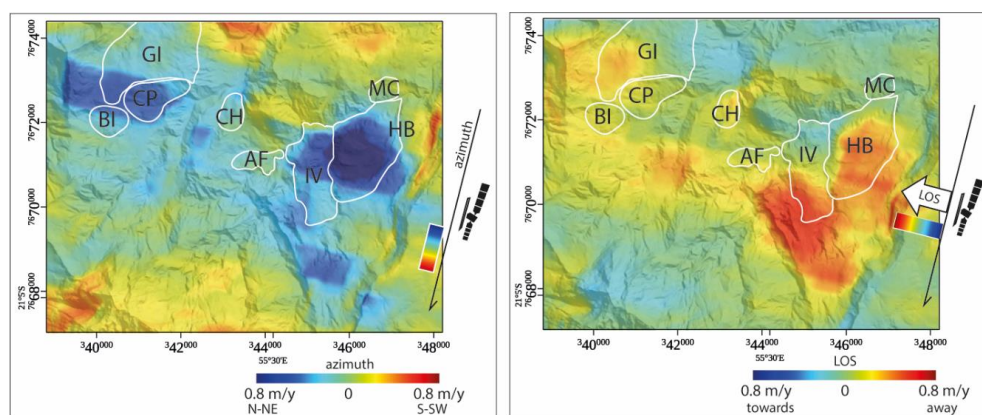
### 222 3.2 Offset tracking Azimuth and Range

223 We show the OT results in Figure 3. Because OT is a subpixel correlation technique, its precision depends on the  
224 image pixel size. Nominally, the correlator implemented into the GAMMA processing chain is as precise as  $1/10^{\text{th}}$   
225 of the pixel size (e.g. Raucoles *et al.*, 2019). Therefore, because the MLI pixel sizes were 8.2 m in the azimuth



226 direction and 7.9 m in the range directions, we can expect precisions of the orders of 0.8 m in a single correlograms.  
 227 Thus, we cannot use OT to measure ground motions smaller than 0.8 m on a single correlogram. The precision  
 228 increases by applying the stacking procedure. Moreover, the stacking procedure can compensate the component  
 229 of the pixel offsets that may be caused by non-zero baselines between Sentinel 1 orbits, which is proportional to  
 230 topography. Furthermore, OT does not have higher limits for ground motion detection. This latter characteristic is  
 231 particularly helpful in CdS, where metric ground motion is expected, particularly within the HB area.

232



233

234

Figure 3. Azimuth (left) and LOS (right) OT velocity maps.

235 The first observation from Figure 3 is that the OT stacking procedure applied to Sentinel 1 MLIs provides  
 236 meaningful results, both in the azimuth and slant range directions. From Figure 3, we find that the fastest ground  
 237 motion in the azimuth direction is localized on the Hell Bourg landslide, N-NW section of the IV landslide, and  
 238 Camp Pierrot (CP) landslide. Ground motion in Hell Bourg can reach 1 m/yr in the azimuth direction. The OT  
 239 signal in the azimuth direction is also visible on a central section of the CP and IV landslides, as fast as 0.7 m/yr.  
 240 In the slant range direction, the OT ground motion signal is localized in the HB landslide, reaching 0.8 m/yr, away  
 241 from the satellite. Figure 3 highlights motion on the S-SE sections of the GI and IV landslides. We also observe  
 242 an unexpected pattern of ground motion S-SE of HB and south of IV, that was consistent with the geomorphology  
 243 of the area but situated in a non-instrumented, uninhabited area on the ground. This signal is intriguing and must  
 244 be validated against *in situ* observations. It might correspond to an area that was considered stabilized or dormant,  
 245 called Crete de Salaze.

246 To further investigate this latter signal, we considered the horizontal component of LOS motion only, combined  
 247 with the azimuth velocities, to extract OT horizontal ground velocities regardless of the motion direction. The  
 248 hypothesis holds in CdS because the horizontal motion (in HB for instance) is almost 7 times larger than the  
 249 vertical velocity. Therefore, we applied :

$$250 \quad |v_h| = \sqrt{AZ^2 + (LOS/\sin i)^2}, \quad (1)$$

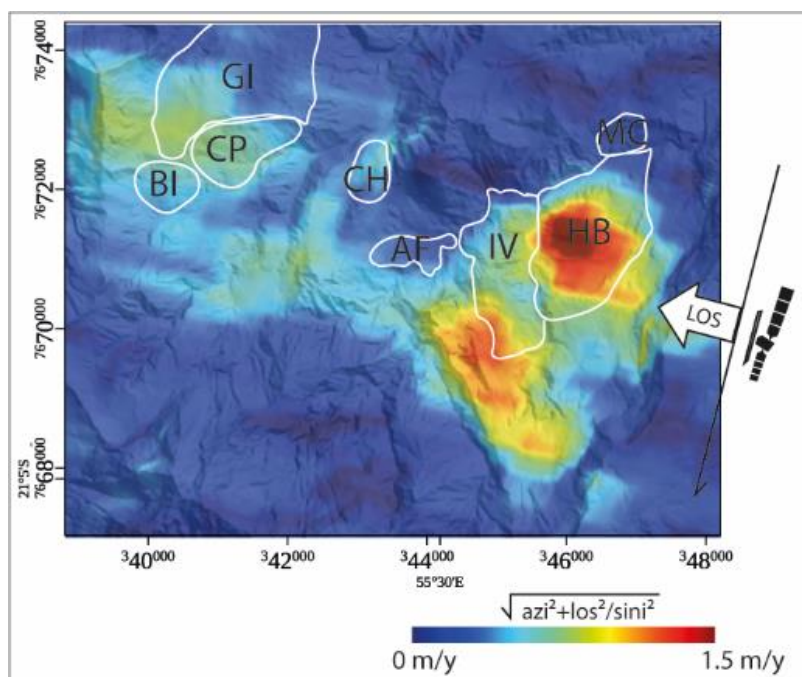
251 to extract the horizontal velocity map,  $|v_h|$ , where  $i$  is the LOS viewing angle ( $37^\circ$  in this case study),  $AZ$  is the  
 252 azimuth offset and  $LOS$  is the range offset (Figure 4). Figure 4 shows that the OT detectable ground motion is  
 253 concentrated in the HB, IV, and south of IV landslides. There is also a weaker but noticeable ground motion signal





254 at the GI and CP landslides. Moreover, there is a marked signal S-SE of IV. This area, considered stabilized or  
255 dormant, must be investigated further, the OT signal may be due to a post cyclonic burst of ground motion.

256



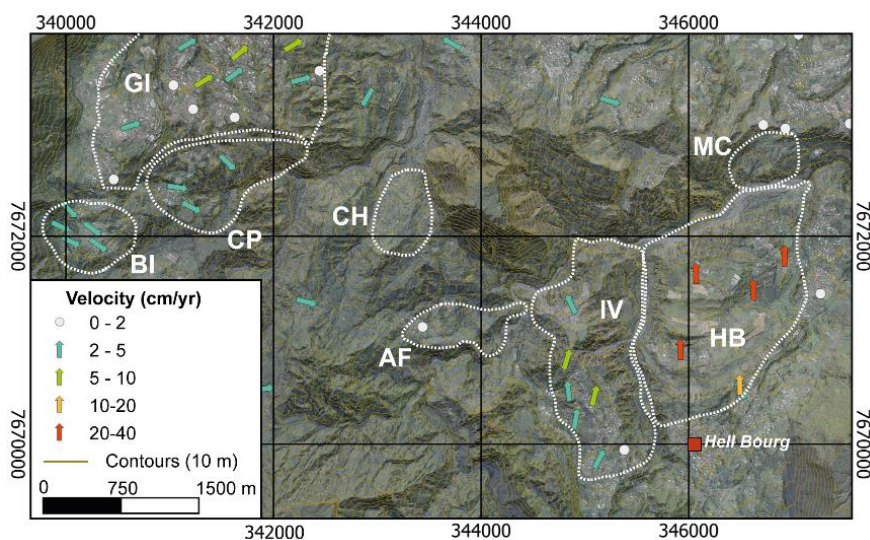
257

258 **Figure 4. Amplitude of the OT horizontal ground velocities independent of direction. We consider only the horizontal**  
259 **component of LOS :  $\sqrt{AZ^2+LOS^2/\sin^2}$ .  $i$  is the LOS viewing angle ( $37^\circ$ ). The hypothesis is that the horizontal motion**  
260 **in CdS (in HB for instance) is almost 7 times larger than the vertical velocity.**

261

#### 262 4. Comparison with global positioning system (GPS) data

263 To gain some insight into the accuracy of SAR velocities maps, we performed a cross-comparison with global  
264 positioning system (GPS) campaigns available at CdS. In this exercise, we compared SAR velocities with GPS  
265 velocities acquired over the time span May 2018 - February 2020. The Global Navigation satellite system (GNSS)  
266 velocities were calculated using 93 geodetic markers across the cirque (Figure 5). They were obtained from the  
267 position of the markers measured with a differential GPS during two campaigns of measurements: May 2018 and  
268 January 2020.



269

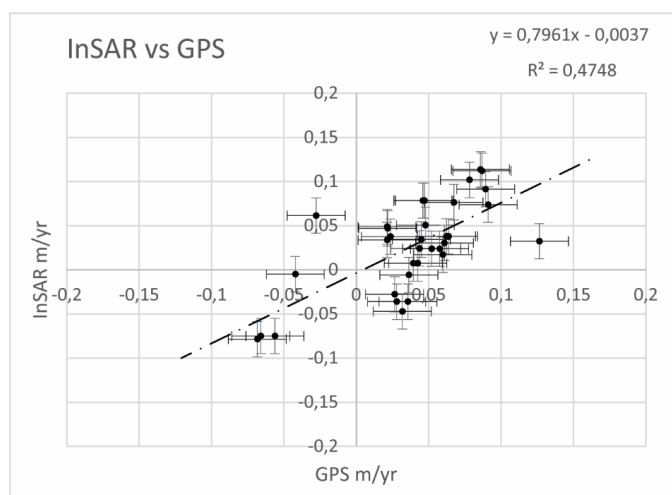
270 **Figure 5. Locations and horizontal velocities of GPS stations. Velocities refers to campaigns in May 2008 and January**  
271 **2020.**

272

273 GPS measurement accuracy varies from one site to another depending on environmental factors (e.g., vegetation,  
274 proximity to buildings, cirque cliffs, and steep ramparts). For each campaign of measurement, the position of a  
275 benchmark was measured four successive times. The final position of the benchmark is the average of these four  
276 measurements. Measurements with deviations of more than 5 cm in altimetry and 3 cm in planimetry were removed  
277 from the dataset. The positioning accuracies are of the order of 2 cm in planimetry and less than 5 cm in altimetry  
278 (Mazué et al., 2013).

279 To compare GPS and SAR velocities (both InSAR and OT), we must project the GPS x, y, and z values into LOS  
280 (= OT range) and OT azimuth direction, by considering that Sentinel 1 had a heading of  $-167.66^\circ$  South with a  
281 look angle of  $36.93^\circ$ . We then obtained  $GPS_{sar}$  values in LOS, range and azimuth direction. Then, we discretized  
282 the  $GPS_{sar}$  values into a number of intervals of 0.03 m width. For each interval, we calculated the median and  
283 identified the geographic location of each point in the interval. At those points, we extracted median  $GPS_{sar}$  and  
284 SAR values. Then, we plotted  $GPS_{sar}$  versus SAR for each interval. The results are scatterplots showing GPS  
285 (LOS) vs InSAR (Figure 6) and GPS (range; azimuth) vs SAR OT (range, azimuth) in Figure 7.

286 From Figure 6, we see that the comparison between InSAR velocities and  $GPS_{sar}$  velocities is satisfactory.  
287 However, there was a general underestimation of motion for the InSAR technique (i.e.,  $InSAR=0.8 \times GPS$ ). This  
288 may be due to an uncompensated residual ramp in the InSAR velocity map.



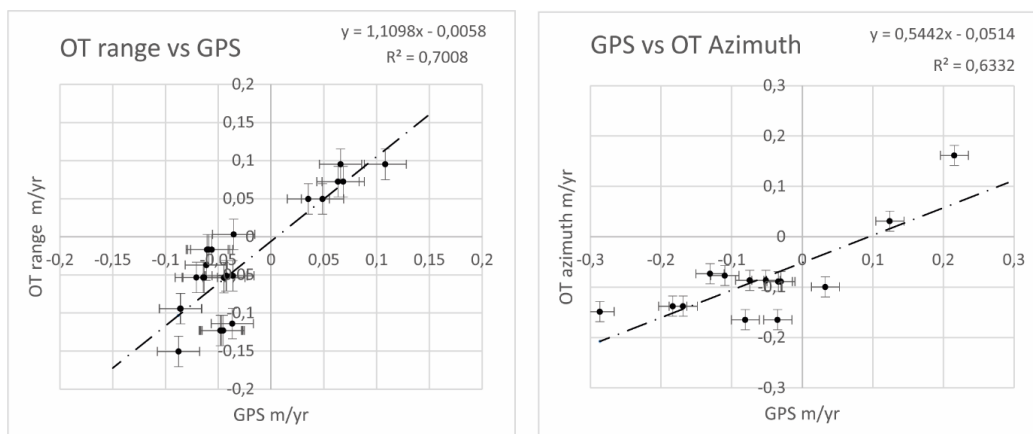
289

290 **Figure 6. InSAR VS GPS (LOS) data (m/yr). InSAR is not sensitive to velocities higher than 2 cm/yr. Therefore, we**  
291 **mask all values that are related to GPS values higher than |2| cm per year.**

292

293 In Figure 7, we show the comparison between  $GPS_{sar}$  and OT velocities in range and azimuth directions. We see  
294 that the comparison between SAR and  $GPS_{sar}$  velocities is good. There is a general underestimation of motion by  
295 the OT technique in the azimuth direction (i.e.,  $OT_{azimuth}=0.5 \times GPS_{sar}$ ). This may be due to an uncompensated  
296 residual ramp in the OTs velocity maps.

297



298

299

300 **Figure 7. Left:  $GPS_{sar}$  vs OT in the range direction (m/yr). Right:  $GPS_{sar}$  vs OT in the azimuth direction (m/yr). Masked**  
301 **GPS values between  $\pm 3$  cm per year**

302



303 **5. Discussion, conclusions, and perspectives**

304 In this study, we applied Sentinel 1 SAR analysis, both InSAR and OT, to the measurement of ground motion on  
305 Cirque de Salazie, Reunion Island, France. Thanks to the high repetition frequency of Sentinel 1, the C-band  
306 InSAR signal was coherent in this region, in contrast with past C-band studies on the study area. This result allows  
307 us to produce interpretable velocity maps, both with InSAR and OT techniques. The InSAR velocity map provided  
308 spatially detailed ground velocities in the LOS of the satellite, with precision reaching a fraction of the SAR  
309 wavelength. The comparison between InSAR and GPS velocities is satisfactory. The Sentinel 1 MLIs OT  
310 technique provided useful measurements. Nevertheless, the comparison between OT and GPS velocities  
311 highlighted several biases that require a more detailed investigation. The biases may be due to a residual orbital  
312 ramp in the OT velocities but also the fact that OT precision is a function of the MLI pixel size. Because the InSAR  
313 and OT techniques provided “relative” measurements, the biases with respect to GPS suggested that absolute  
314 calibration of SAR maps is needed to compare SAR and GPS results.

315 Within the InSAR and OT detection limits and the period of SAR measurements (October 2017–November 2018)  
316 this study displayed the ground motion and internal kinematics on HB landslide, the N-NW section of IV landslide,  
317 and CP landslide. Moreover, we point out an unexpected pattern of ground motion S-SE of HB and South of IV,  
318 consistent with the geomorphology of the area but situated in a non-instrumented, uninhabited area on the ground.  
319 We suggest that it might correspond to an area that was considered stabilized or dormant, called Crete de Salaze.  
320 Motion in this area might have been reactivated as a consequence of heavy rainfall and thus represents a post  
321 cyclonic burst of ground motion.

322 Three GPS sites on the South-Western part of IV landslides indicates ground motion in this sector of CdS.  
323 Therefore, this noticeable signal requires further consideration and investigation.

324 We need precise time series of this ground motion, localized on those three specific areas, to discriminate whether  
325 we can highlight rheological changes due to the post-cyclonic activity.

326 There are rooms for methodological improvement:

327 Even though the Sentinel 1 ascending mode is less adapted in CdS due to shadow and layover effects depending  
328 on the look angle, it may be possible to exploit the few coherent pixels to extract the vertical and east-west  
329 components of ground displacement, by a combination of Sentinel 1 InSAR in ascending and descending modes.  
330 The exploitation of both InSAR and OT from Sentinel 1 and other SAR missions (e. g. ALOS 2, TerraSAR X)  
331 would improve data coverage, spatially and temporally. OT with Sentinel 1 data revealed precious to measure  
332 large ground motion in CdS. In this study, we calculated OT on MLIs 3-2; we could run an experiment to determine  
333 whether OT from MLIs 2-1 or even MLIs 1-1 could lead to more accurate results.

334 In conclusion, Sentinel 1 InSAR and OT present high potential for routine monitoring on CdS, as a complement  
335 to *in situ* techniques (i e., Rault et al., 2022). This study presented a solid premise for the future exploitation of the  
336 European Ground Motion Service (EGMS) of the European Union Copernicus program, based on Sentinel 1  
337 InSAR, in CdS.

338



339 **References**

- 340 Aslan, G., Fomelis, M., Raucoules, D., De Michele, M., Bernardie, S., and Cakir, Z.: Landslide Mapping and  
341 Monitoring Using Persistent Scatterer Interferometry (PSI) Technique in the French Alps. *Remote Sens.*, 12, 1305,  
342 <https://doi.org/10.3390/rs12081305>, 2020.
- 343 Belle, P., Aunay B., Bernardie, S., Grandjean, G., Ladouche, B., Mazué, R., and Join, J-L.: The application of an  
344 innovative inverse model for understanding and predicting landslide movements (Salazie cirque landslides,  
345 Reunion Island). *Landslides*, 11, 343–355, 2014.
- 346 Costantini, M.: A novel phase unwrapping method based on network programming. *IEEE Trans. Geosci. Remote*  
347 *Sens.*, 36, 3, 813–821, 1998.
- 348 Delacourt, C., Raucoules, D., Le Mouélic, S., Carnec, C., Feurer, D., Allemand, P., and Cruchet, M.: Observation  
349 of a Large Landslide on La Reunion Island Using Differential Sar Interferometry (JERS and Radarsat) and  
350 Correlation of Optical (Spot5 and Aerial) Images. *Sensors*, 9(1), 616-630, 2009.
- 351 de Michele, M., and Briole, P.: Deformation between 1989 and 1997 at Piton de la Fournaise volcano retrieved  
352 from correlation of panchromatic airborne images. *Geophys. J. Int.*, 169(1), 357–364, *doi:10.1111/j.1365-*  
353 *246X.2006.03307.x.*, 2007.
- 354 de Michele, M., Raucoules, D., Lasserre, C., Pathier, E., Klinger, Y., Van Der Woerd, J., de Sigoyer, J., and Xu,  
355 X.: The  $M_w$  7.9, 12 May 2008 Sichuan earthquake rupture measured by sub-pixel correlation of ALOS PALSAR  
356 amplitude images. *Earth Planet Space*, 62, 875–879, <https://doi.org/10.5047/eps.2009.05.002>, 2010.
- 357 de Michele, M., Raucoules, D., de Sigoyer, J., Pubellier, M., and Chamot-Rooke, N.: Three-dimensional surface  
358 displacement of the 2008 May 12 Sichuan earthquake (China) derived from Synthetic Aperture Radar: evidence  
359 for rupture on a blind thrust. *Geophysical Journal International*, 183, 3, 1097–1103, <https://doi.org/10.1111/j.1365->  
360 *246X.2010.04807.x.*, 2010.
- 361 Doubre, C., Déprez, A., Masson, F., Socquet, A., Lewi, E., Grandin, R., and Abayazid, A. : Current deformation  
362 in Central Afar and triple junction kinematics deduced from GPS and InSAR measurements. *Geophysical Journal*  
363 *International*, 208(2), 936-953. doi: 10.1093/gji/ggw434, 2017.
- 
- 364
- 365 Le Bivic, R., Allemand, P., Quiquerez, A., and Delacourt, C. : Potential and Limitation of SPOT-5 Ortho-Image  
366 Correlation to Investigate the Cinematics of Landslides: The Example of “Mare à Poule d’Eau” (Réunion, France).  
367 *Remote Sensing*, 9(2), 106, <https://doi.org/10.3390/rs9020106>, 2017.
- 
- 368
- 369 Massonnet, D., and Feigl, K.: Radar interferometry and its application to changes in the Earth's surface. *Rev.*  
370 *Geophys.*, 36, 4, 441, 1998.
- 371 Mazué, R., Aunay, B., and Belle, P. (2013). Suivi des réseaux géodésiques dans les cirques de La Réunion.  
372 Rapport BRGM No. RP-61994-FR – p. 66. Available at <http://infoterre.brgm.fr/rapports/RP-61994-FR.pdf>



- 373 Michel, R., and Rignot, E.: Flow of Glaciar Moreno, Argentina, from repeat-pass Shuttle Imaging Radar images:  
374 a comparison of the phase correlation method with radar interferometry. *J. Glaciol.* 45, 93-100, 1999.
- 375 Michel, R., Avouac, J. P., and Taboury, J.: Measuring ground displacements from SAR amplitude images:  
376 Application to the Landers earthquake, *Geophys. Res. Lett.*, vol. 26, no. 7, pp. 875–878, Apr. 1999.
- 377 Raucoules, D., Bourguin, B., de Michele, M., Le Cozannet, G., Closset, L., et al. : Validation and intercomparison  
378 of Persistent Scatterers interferometry: PSIC4 project results. *Journal of Applied Geophysics*, 68 (3), 335-347,  
379 2009.
- 380 Raucoules, D., Tomaro, F., Foumelis, M., Negulescu, C., de Michele, M., and Aunay, B. : Landslide Observation  
381 from ALOS-2/PALSAR-2 Data (Image Correlation Techniques and Sar Interferometry). Application to Salazie  
382 Circle Landslides (La Reunion Island). *IGARSS 2018 – 2018 IEEE International Geoscience and Remote Sensing*  
383 *Symposium*, Jul 2018, Valencia, France. pp.506-509, 10.1109/IGARSS.2018.8517998, hal-02734613.
- 384 Raucoules D., de Michele, M., and Aunay, B.: Landslide displacement mapping based on ALOS-2/PALSAR-2  
385 data using image correlation techniques and SAR interferometry: Application to Salazie Circle landslides (La  
386 Réunion Island). *Geocarto International*, 35, 113-127, 2020.
- 387 Raucoules, D., Le Cozannet, G., de Michele, M., and Capo, S.: Observing water-level variations from space-borne  
388 high-resolution Synthetic Aperture Radar (SAR) image correlation, *Geocarto International*, 33(9), 977-987, 2018.
- 389 Raucoules, D., de Michele, M., Mazué, R., and Aunay, B.: MvTerre-2 : Observation de mouvements de terrain  
390 sur le cirque de Salazie à partir de mesures de télédétection radar satellitaire, *Rapport BRGM RP- 61187-FR*, 51  
391 p. Available at <http://infoterre.brgm.fr/rapports/RP-61187-FR.pdf>, 2016.
- 392 Raucoules, D., de Michele, M., Malet, J-P., and Ulrich, P.: Time-variable 3D ground displacements from high-  
393 resolution synthetic aperture radar (SAR). Application to La Valette landslide (South French Alps), *Remote*  
394 *Sensing of Environment*, 139, 198-204, 2013.
- 395 Rault, C., Thiery, Y., Chaput, M., Reninger, P. A., Dewez, T. J. B., Michon, L., and Aunay, B.: Landslide Processes  
396 Involved in Volcano Dismantling From Past to Present: The Remarkable Open-Air Laboratory of the Cirque de  
397 Salazie (Reunion Island). *Journal of Geophysical Research: Earth Surface*, 127(5), e2021JF006257, 2022.
- 398 Strozzi, T., Luckman, A., Murray, T., Wegmuller, U., and Werner, C.L.: Glacier motion estimation using SAR  
399 offset-tracking procedures, *IEEE Transactions on Geoscience and Remote Sensing*, 40, 11, 2384 - 2391, 2002.
- 400 Tulet, P., Aunay, B., Barruol, G., Barthe, C., Belon, R., Bielli, S., and Vèrèmes, H.: ReNovRisk: a multidisciplinary  
401 programme to study the cyclonic risks in the South-West Indian Ocean. *Natural Hazards*, 107(2), 1191-1223, 2021.